Development of a valve-regulated lead−acid battery with thin tubular positive plates for improved specific energy and optimization for low charge-factor operation

I. Dyson[*], Paul Griffin

CMP Batteries Ltd., P.O. Box 1, Salford Road, Over Hulton, Bolton BL5 1DD, UK

Abstract

An overview of the design and development of a valve-regulated lead–acid (VRLA) battery with thin tubular plates is presented. Substantially improved specific energy in driving-cycle tests shows how the strategy of increasing the number of plate couples through the production of plates with component thicknesses that are 50% of those for existing technology plates is effective in meeting the requirements of the target application. Exploring the possibilities for removing inactive materials shows how reducing spine material to an extent limited to maintenance of an acceptable metal/active-material surface ratio ('gamma' value) by using an elliptical spine is effective, but that further reductions impair cell performance on cycling. Matching recharge characteristics with cell design and controlled initial electrolyte of the cells is discussed in terms of the influence of the oxygen-recombination rate on the recharge response. Changes during stable operation are illustrated in terms of charge response data during long cycle-life with 80% depth-of-discharge and a low, overcharge, viz., 4% C_5. With an appropriate alloy, thin spines remain intact after more than 1000 cycles of service. Growth and non-penetrating corrosion rates are low for the optimized operating conditions.

1. Background

Lead–acid batteries with tubular positive plates have long cycle-lives, but high-rate performance for electric vehicle (EV) applications has been limited by the consequences of a relatively large plate-couple pitch on impedance and current density. When using pressure-diecast lead-alloy spines instead of grids, tubular positive plates display higher resistance to corrosion because: (i) high quality, defect-free castings are easily manufactured; (ii) the components are not exposed to stress corrosion to the same extent as with grids, where the growth of horizontal as well as vertical wires results in substantial complex forces at the points of intersection. More relevant to the valve-regulated lead−acid (VRLA) battery is the fact that the positive active-material is contained in a tubular fabric gauntlet and so loss of discharge capacity through softening and shedding of the this material can be prevented. Such degradation results in low cycle-life

with pasted-plate VRLA batteries unless the material has a high paste density and is effectively supported by a high-performance separator in combination with high plate-group pressure ('compression').

The objective of the work reported here is to develop a VRLA battery with tubular positive plates that is optimized for high specific energy and good cycle-life. This objective is pursued by the extension of present commercial technology to progressively thinner plates with pressure-diecast spines. Increase in positive-plate utilization is attempted by reducing the grid mass, and by adopting alloys with improved corrosion resistance, creep strength and resistance to the development of high impedance at the spine–active-material interface.

1.1. Raising positive-plate performance

The performance of positive active-material may be improved, subject to electrolyte availability, by reducing the thickness of the material, which follows from a decrease in plate thickness. Improved performance may also be sought through reduction in the density of the active-material.

[*] Corresponding author. Tel.: +44-1204-661359;
fax: +44-1204-659806.
E-mail address: dysoni@cmpbatteries.co.uk (I. Dyson).

In terms of performance and cycle-life, the process is already optimized for existing products and their established applications. For thin plates and high-rate discharge duties associated with EV applications, it may be possible to increase plate specific energy by reducing the density of the positive active-material without detriment to cycle-life.

The specific energy of positive plates may be further increased by decreasing the amount of inactive components. Whilst not participating in the energy-conversion reactions, grids and spines do contribute to performance and life through providing electronic conductivity and by mechanically supporting the active mass. Pavlov [1] has studied the influence of (i) the grid corrosion layer and (ii) the inner active material (that contributes to conductivity with the bulk active material) on the premature capacity loss of positive plates, especially those with low-antimony or antimony-free grid alloys. It was found that the ratio of the active-material mass to the area of the grid–active-material interface is an important characteristic. This ratio, which is called 'gamma' and is expressed in $g\,cm^{-2}$, should be kept low for good cycle-life. With a design value of $0.8\,g\,cm^{-2}$, acceptable cycle-life may be achieved with antimony-free alloys, but with higher values, capacity may decline.

The spine mass may be decreased either by using less spines in a plate of given width, or by reducing the cross-sectional area of the spines. Plate performance at high rates will be influenced by the change in resistive voltage drop along the spines. Maintenance of available capacity, i.e. cycle-life, may be impaired by reduction of the spine–active-material area relative to the active mass. The influence of the two approaches, viz. spine number or cross-sectional area, on electrical resistance and gamma are reviewed in Fig. 1 for a cell of 27 spines of 1.9 mm diameter. For variation of spine mass, the data indicate relative values of electronic resistance, gamma response for reduction by spine diameter, gamma response for reduction by spine number, and equivalent spine diameter. The resistance increases as the spine mass is reduced, irrespective of the method. For any reduced relative spine mass, the increase in gamma is greater if the spine number is reduced than if the spine cross-sectional area is reduced. Taking advantage of an improved alloy [2], the influence on gamma has been decreased in approaches to removing lead by adopting an elliptical spine section to enhance the surface area relative to the mass.

1.2. Charging and related design aspects

The influence of the oxygen-recombination cycle on the charging of VRLA batteries has been described by Berndt [3]. In standby and float applications, charging is optimized to maintain the state-of-charge of the active materials, which otherwise would decrease mainly through self-discharge reactions. Batteries and charging may be optimized for low daily and cumulative overcharge that amounts to less than 1% of nominal capacity per day. By virtue of the 'oxygen cycle', this is achieved with high recombination efficiency and negligible water loss. In cycling applications, however, overcharge has to be given, not necessarily on every cycle but at least regularly in order to recharge the electrodes under conditions where the competing gassing reactions are accelerated. For cycling service, the charging schedules recommended by VRLA battery manufacturers result in more than 10% overcharge per cycle.

In flooded cells, charging of the negative plate is more efficient than that of the positive and, if stratification is controlled, the state-of-charge of both electrodes can be maintained by applying as little as 4% overcharge per cycle. In VRLA batteries, the effective overcharge of the negative
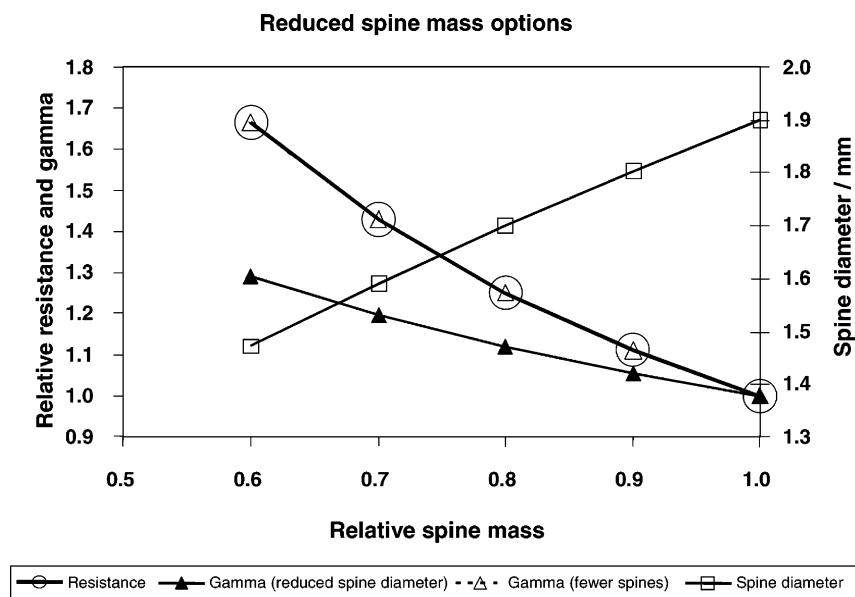

Fig. 1. Influence of reduced spine mass (by spine diameter and number) on spine resistance and gamma (ratio of positive active-material (g) to spine surface area (cm^2)).
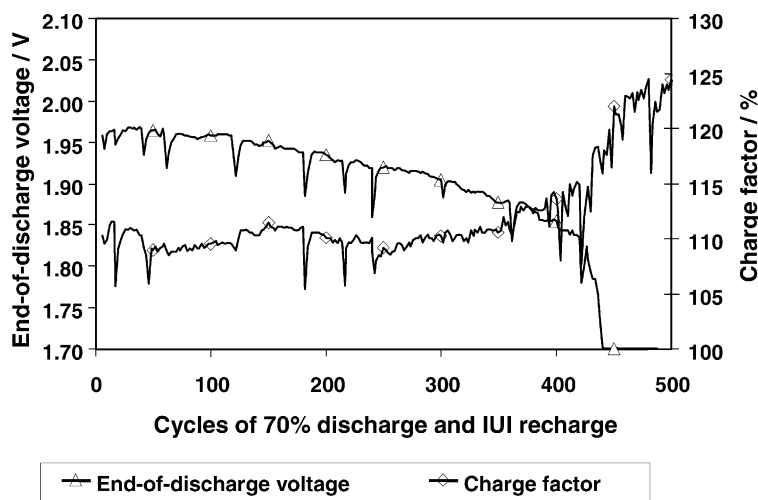
Fig. 2. Effect of increasing charge factor on battery failure after starting life with high electrolyte saturation.

plates is diminished by oxygen-recombination. Under careful control, this means that it is possible to have the positive and negative plates approach complete recharge together. With high rates of oxygen-recombination, the state-of-charge of the negative plate may decline with charging conditions that are sufficient for the positive plates.

Providing that electrolyte stratification, electrode degradation and passivation are controlled, the optimum cycle-life of VRLA batteries is dependent on providing just sufficient charge to maintain the state-of-charge of the active materials, whilst avoiding excessive water loss and grid corrosion. If there is insufficient charge, performance will decline with state-of-charge.

Excessive overcharge results in water loss and increased working temperature. The rate of oxygen-recombination increases as the saturation of the separator with electrolyte is reduced. As water is lost with successive cycles, the increased oxygen-recombination rate reduces the effective overcharge for the negative plates, and hence their state-of-charge may decline. This situation is characterized, after relatively stable operation, by an increase in the charge factor and reduction of available capacity. This is illustrated in Fig. 2 which shows data for a charge regime with a relatively high charge factor and cells which initially have a low oxygen-recombination rate. Failure is accelerated by increasing oxygen-recombination rate, charge factor and working temperature.

The strategy for ensuring good cycle-life in the present study is to control, through electrolyte saturation, the initial oxygen-recombination rate so that both electrodes approach charge together at a low, but sufficient, overcharge. With this approach, water loss, particularly early in life, should be minimal and the cell response to the charging regime should remain stable over a large number of cycles. Extended maintenance of capacity would compensate for any reduction of initial capacity due to lowering of the electrolyte saturation.

1.3. Raising negative-plate performance

In addition to improved formulation and mass balance, to be identified in a matrix test, the performance of the negative plate may be improved by a reduction in grid mass. Approaches include the use of thin grids and large pellets (50% of grid mass is in the mesh). The conductivity of discharged negative active-material should support large pellets, especially with good separator support, but this approach may not be appropriate if structure of the material degrades with EV cycles. Negative plates with large pellets have been included in a preliminary study of negative-plate design without limitation of performance or life under driving-cycle tests with existing technology positive plates.

2. Experimental

2.1. Couple design

In addition to evaluating the degree of increased plate utilization through reduction in relative spine mass, it was decided to seek high battery power by making a further reduction in plate pitch in order to reduce cell impedance.

A design model, which ignores any 'remote' electrolyte, has been developed to facilitate active-material balancing for different group dimensions. The 'nominal' design uses an established good balance of conservative active-material utilizations, which provides scope to enhance each without early limitation by others. Component thicknesses have been adjusted to balance positive plate, negative plate and acid calculated capacities with active-material loadings at 14 and 12 g Ah^{-1}, and a relative density (rel. dens.) on discharge of 1.300–1.100, respectively. These features promise a 20% enhancement in performance through increased active-material utilizations which arise from the reduced diffusion distances for the thinner-plate couples, probably with a

Table 1
Rectangular EV tubular plates: nine-plate construction for 50.3 mm cell length and 145 mm gauntlet height (dimensions in mm)

Design parameter	3ET205 translation		80% spine area		80% spine number	
	Round RMDR1	Ellipse RMDR0	Round RMDR2	Ellipse RMDR3	Round RMDR11	Ellipse RMDR12
Spines (number)	25	25	25	25	20	20
Spines (major diameter)	1.90	3.00	1.70	2.41	1.90	3.00
Spines (minor diameter)	1.90	1.20	1.70	1.20	1.90	1.20
Tube inside width	4.88	4.88	4.88	4.88	6.36	6.36
Positive thickness	4.850	4.850	4.775	4.775	4.650	4.650
Negative thickness	2.375	2.375	2.400	2.400	2.425	2.425
Capacity (Ah)	70.5	70.5	71.3	71.3	72.0	72.0
Gamma (g cm^{-2})	1.22	1.02	1.38	1.24	1.56	1.30

lower acid relative density at end of discharge. Further improvements were anticipated for operation with increased acid relative density on charging.

The design data for positive active-material balance in cells of various selected dimensions are presented in Tables 1–3 for increasing couple numbers. Design data, which are based on scaling-down existing couple technology according to established design rules, are presented in the first two columns. The other columns show designs with 20% decrease in spine mass by reduction in spine cross-sectional area and then by reduction in the number of spines and tubes. Design data are included for round spine sections, as well as for an ellipse of equivalent area which gives a

reduced value of gamma. The 3ET205, high specific energy, flooded monobloc with tubular positive plates, which has proved popular in EV applications, is used as the design basis. Data for the design based on translation of this battery to an AGM product with rectangular tube sections are shown in Table 1. Corresponding data for 'thin' tubular plates (one extra couple) and 'thinner' tubular plates (two extra couples) in the same cell container are given in Tables 2 and 3, respectively.

A 20% reduction in gamma is obtained when elliptical spine sections are used (Table 1). Because the minor diameter is held at 1.2 mm as a processing limit, the advantage is reduced for designs with 80% spine area as the aspect

Table 2
Thin tubular plates: 11-plate construction for 50.3 mm cell length and 145 mm gauntlet height (dimensions in mm)

Design parameter	Thin plate		80% spine area		80% spine number	
	Round RMDR6	Ellipse RMDR7	Round RMDR4	Ellipse RMDR5	Round RMDR8	Ellipse RMDR9
Spines (number)	25	25	25	25	20	20
Spines (major diameter)	1.73	2.49	1.56	2.03	1.73	2.49
Spines (minor diameter)	1.73	1.20	1.56	1.20	1.73	1.20
Tube inside width	4.88	4.80	4.88	4.88	6.36	6.36
Positive thickness	4.050	4.050	3.975	3.975	3.875	3.875
Negative thickness	1.925	1.950	1.950	1.950	1.975	1.975
Capacity (Ah)	70.0	70.0	70.5	70.5	71.3	71.3
Gamma (g cm^{-2})	1.07	0.95	1.20	1.12	1.36	1.21

Table 3
Thinner tubular plates: 13-plate construction for 50.3 mm cell length and 145 mm gauntlet height (dimensions in mm)

Design parameter	Thinner plate		80% spine area		80% spine number	
	Round RMDR13	Ellipse RMDR14	Round RMDR15	Ellipse RMDR16	Round RMDR17	Ellipse RMDR18
Spines (number)	25	25	25	25	20	20
Spines (major diameter)	1.64	2.24	1.47	1.80	1.64	2.24
Spines (minor diameter)	1.64	1.20	1.47	1.20	1.64	1.20
Tube inside width	4.88	4.88	4.88	4.88	6.36	6.36
Positive thickness	3.500	3.500	3.425	3.425	3.350	3.350
Negative thickness	1.625	1.625	1.650	1.650	1.675	1.668
Capacity (Ah)	69.0	69.0	69.5	69.5	70.3	70.3
Gamma (g cm^{-2})	0.93	0.85	1.04	1.00	1.18	1.08

ratio of the ellipse is lower. For the same reason, the reduction in gamma for an elliptical spine section is less for the thin and the thinner plates (Tables 2 and 3), namely, 12 and 9%, respectively. Elliptical-section spines are used for the development designs. At the proposed aspect ratio, these spines appear to present little additional processing difficulty and have the potential advantage of a lower gamma.

For the thinner-plate, option RMDR14 with no additional spine reduction was adopted. Given the possibility of processing problems with such thin positive plates and also the potential to alter the tooling to produce a 25-spine thin plate (design RMDR7 or RMDR5) and the opportunity to test the influence of gamma, the 20-spine RMDR9 version was selected as the thin-plate design instead of the 25-spine RMDR5, despite its low gamma.

Existing standard and high specific energy products have positive active-material section and internal tube dimensions of 7.2 mm × 6.4 mm and 6.6 mm × 4.7 mm, respectively. The corresponding development design dimensions of 6.4 mm × 3.1 mm and 5.7 mm × 2.7 mm, reflect a substantial reduction in the thickness of the positive active-material. Summaries of two 'nominal' cell designs—a thin plate version with 11 plates in a 50.3 mm container and a thinner-plate version with 13 plates—are listed in Table 4. As a basis for optimising performance, tests were conducted on cells that included a range of design and process variables. A test matrix, which included reduced positive active-material density and negative paste as variables in combination with electrolyte/separation, was tested according to the EUCAR

ECE15L [4] driving-cycle test. The schedule is based on specific power and is described in Section 2.3, below, and illustrated later in Fig. 6.

2.2. Component processing and test cell build

2.2.1. Processing

With the exception of the positive plates, component processing was not expected to present any problems. Although the negative plates are thin compared with those in existing motive-power products, their dimensions are typical of those in other lead–acid product ranges. The tubular positive plates are, however, substantially thinner than those for existing products.

The dimensions of the pressure-diecast spines were smaller than the minimum recommended by the manufacturer of the casting machine and dies. Nevertheless, castings of good quality were produced in a lead−calcium−high tin (1.2 wt.%) alloy, without any great difficulty. For the initial production, handling was facilitated by hanging the untrimmed castings overnight to age-harden before cropping and threading the spines into gauntlets. No other processing concession was necessary.

Plates were filled with the positive active-material precursor using the filter-fill process; an aqueous suspension was injected at pressure so that water filtered through the gauntlet fabric. Since plate thickening through distortion (inflation) of the rectangular tubes was anticipated as a potential problem for the thin plates; expansion control was sought through the addition of a perforated restraining mesh to the filling module.

The thin tubular and pasted negative plates were prepared according to the present process specifications of CMP Batteries Ltd., except that instead of drying in an inert gas oven, electro-formed negative plates were vacuum dried in small batches.

2.2.2. Cell performance test—electrolyte saturation

In order to gauge the influence of electrolyte saturation on the performance and the charge response of the new designs, the quantity of electrolyte addition was varied to reflect a range of separator saturations using an additional series of cells. Cell PNH has positive and negative plates which are processed to 'nominal' specifications; filling with 1050 g of 1.280 rel. dens. sulfuric acid equated to saturated separators. For cell PNJ, filling with 1000 g of 1.280 rel. dens. sulfuric acid equated to 92% saturated separators, and for PNK, filling with 950 g of 1.280 rel. dens. sulfuric acid equated to 84% saturated separators.

2.2.3. Cell performance testing—design matrix test—optimizing the active-material balance

The cell and battery designs were optimized according to the results of performance testing a matrix of design and process variables. Three variations of positive plate, negative plate and separator/electrolyte were combined.

Table 4
Design characteristics of the two 'nominal' cell designs

Group design	Thin-plate couple	Thinner-plate couple
Cell width (mm)	157	157
Cell length (mm)	50.3	50.3
Positive plates	5	6
Tube inside dimensions (mm)	6.36 × 3.08	4.89 × 2.70
Spine ellipse (mm)	2.49 × 1.20	2.24 × 1.20
Spine number	20	25
Spine pitch (mm)	7.36	5.89
Gauntlet height (mm)	145	145
Plate height (maximum, mm)	156	156
Plate width (mm)	151	151
Plate thickness (mm)	3.88	3.50
Negative plates	6	7
Plate thickness (mm)	1.98	1.63
Grid thickness (mm)	1.78	1.43
Plate height (mm)	149	149
Plate width (mm)	151	151
Horizontal wire pitch (mm)	8	8
Vertical wire pitch (mm)	18	18
AGM compressed thickness (mm)	0.90	0.72
AGM thickness at 10 kPa (mm)	1.12	0.89
Grammage (g m^{-2})	178	141

Table 5
Cell build plan and codes

Design aspect	Code	Description
Positive-plate variants	P/S	Regular fill
	Q/T	Medium density
	R/U	Low density
Negative-plate variants	N	Regular pasting
	M	Flush pasting
	L	Low paste density
Separator and electrolyte variants	E	Normal plate wrap, 1.300 rel. dens.
	F	Positive plate wrap, 1.300 rel. dens.
	G	Normal plate wrap, 1.320 rel. dens.

rel. dens.: relative density.

Relative to the nominal design, additional plate related factors were:

- positive active-material reductions of 7.5 and 15% by changing the filling slurry formulation;
- negative active-material reductions by under-pasting and by using a paste of lower density.

Electrolyte/separator variables were:

- plate wrap, 1.300 rel. dens. electrolyte (both positive and negative plates were 'U' wrapped);
- plate wrap, 1.320 rel. dens. electrolyte (with AGM separator);
- positive plate wrap, 1.300 rel. dens. electrolyte (positive plate only 'U' wrapped with thicker AGM).

The test plan for cell build combined all the variables presented in Table 5 and was duplicated for the 11- and 13-plate couples that were distinguished by using different code letters for their positive-plate variants, i.e. P, Q and R for the 11-plate design with thin tubular positive plates and S, T and U for the 13-plate design using thinner tubular positive plates.

2.2.4. Electrolyte saturation

The calculated 'just saturated' electrolyte volume was checked by filling trials with additional test cells for each combination of plate and separator variables. The cells were weighed, slightly overfilled with electrolyte, drained of free electrolyte, and re-weighed to establish the quantity of electrolyte that saturated the cell group. Using the cell design model to calculate this quantity, the test cells were each filled with electrolyte sufficient to give 5% under-saturation of the compressed AGM separator when positive and negative active-materials were saturated. Wherever a target saturation other than 95% was used, the stated saturation was controlled on the same basis.

2.2.5. Cell mass

Where mass was used to determine the discharge rate or power, or to calculate the specific energy, that mass was

based on one-sixth of the design battery container, lid and top-lead mass plus the variant-average plate, separator and electrolyte masses.

2.3. Prototype cell performance testing

After vacuum filling with weighed quantities of electrolyte, the following sequence was followed.

2.3.1. Individual cell performance testing

- Initial charge: stepped constant current to 2.45 V plus 40% C_5 at 6% C_5 A at 25 °C.
- Measured 5-h rate discharge, rated at 70 Ah, and recharge to +25% C_5 at 25 °C.
- Seven conditioning cycles of 75% discharge and recharge to +20% C_5 at 25 °C.
- Measured 5-h rate discharge, rated at 70 Ah, and recharge to +20% C_5 at 25 °C.

2.3.2. Six-cell string testing at 23 °C (EUCAR)

- Measured 5-h rate discharge, rated at 70 Ah, and recharge at 23 °C.
- Discharge under ECE15L profile (see Table 6) and recharge at 23 °C.
- Measured 5-h rate discharge, rated at 70 Ah, and recharge at 23 °C.

Table 6
EUCAR ECE15L discharge profile

Time (s)	W kg^{-1}
Urban part of ECE15-L	
0–11	0.0
11–15	11.1
15–23	2.0
23–28	−2.8
28–49	0.0
49–61	18.2
61–85	5.1
85–96	−5.6
96–117	0.0
117–143	23.2
143–155	10.5
155–163	−8.5
163–176	5.8
176–188	−6.2
188–195	0.0
Suburban part of ECE15-L	
0–20	0.0
20–61	32.8
61–111	20.1
111–119	−16.0
119–88	10.4
188–201	47.9
201–251	20.1
251–275	51.9
275–358	35.4
358–380	−20.7
380–400	0.0

- Discharge under ECE15L profile and recharge at 23 °C.
- Measured 5-h rate discharge, rated at 70 Ah, and recharge at 23 °C.
- Discharge under ECE15L profile and recharge at 23 °C.

2.3.3. Six-cell string testing at 30 °C

- Discharge at 14.0 A (5-h rate discharge for 70 Ah) and recharge.
- Discharge at 20.8 A (3-h rate discharge for 70 Ah) and recharge.
- Discharge at 28.38 A (2-h rate discharge for 70 Ah) and recharge.
- Discharge at 46.9 A (1-h rate discharge for 70 Ah) and recharge.
- Discharge at 75.6 A (30-min rate discharge for 70 Ah) and recharge.

The EUCAR ECE15L discharge profile repeats two sequences of the 195-s Urban Part and one of the 400-s Suburban Part until the demand cannot be met with a minimum terminal voltage of 1.5 V per cell.

2.4. Cycle testing to 80% depth-of-discharge

The recharge responses of small tubular-plate cells may differ from their larger counterparts. The return of charge, with the same charging characteristic, appears to be lower with the smaller cells, this is probably as a consequence of the different thermal characteristics. It is difficult to reconcile an overcharge per cycle of 8% C_5, 12% C_5 or more for 'maintenance-free' VRLA batteries when the capacity of their flooded counterparts can be sustained for over 2000 cycles with only 4% C_5 per cycle, provided that electrolyte stratification is controlled. Extensive testing may be necessary to establish the appropriate charge regime for these new tubular designs; preliminary tests have compared constant current and taper charge initial phases with 4 and 6% C_5 overcharge per cycle. Application of the taper charge characteristic has failed to enhance cycle-life and the results are not presented here.

The IUI charging consists of three phases: (i) charging at a constant current which may be expressed, relative to nominal capacity, as A/100 Ah or as a numerical percentage of capacity, expressed in % C_5 A and which is terminated when the average cell voltage rises to limit; (ii) charging with controlled voltage until the current falls to that of the final, constant-current phase; (iii) constant-current charging which is terminated to give an appropriate overcharge or charge factor for the application. C_5 is the nominal 5-h discharge capacity. At the start of testing, IUI schedules had an initial current limit of 20% C_5 A with a voltage limit of 2.35 V per cell to the second constant-current rate of 1.6% C_5 A, and were terminated after 4 or 6% C_5 overcharge. The measured capacities of prototype cells were generally higher than the design capacity of 70 Ah. For cycle tests, cells were rated at 80 Ah and discharged to 80% of that nominal capacity.

When, in these and other tests, it was established that the capacity of thin-plate designs of cell was not sustained by 4% C_5 overcharge, but was by 6% C_5 overcharge, the charge factor of the test regime was amended to 6% C_5. Some cycles were performed with partial-state-of-charge (PSoC) operation by omitting the second constant-current phase. In PSoC operation, a sequence of two cycles of IU recharge, i.e. without the second constant-current phase, and one cycle with IUI charging was continually repeated. Because the capacity of the thinner plates was sustained by 4% C_5 overcharge, the test with a high charge factor was changed to the PSoC regime.

Meissner et al. [5] have described how the available capacity of batteries is influenced by the discharge duty and the charging method that is applied. In brief, the capacity declines to a lower value for successive cycles at high rates of discharge, but increases to a higher level for successive cycles at low rates of discharge. When the initial charging rate is varied, the available capacity is higher when charging with a high initial rate than with a low initial rate. The capacity that is reduced in this manner is found to recover after periods at open-circuit. This characteristic is reported to be weak with high-antimonial positive grid alloys, increases with low-antimony alloys, and occurs most strongly in cells with antimony-free alloys.

Thin-plate cells—but not thinner-plate cells—suffer from declining capacity with successive cycles. The capacity can be recovered, however, by imposing rests between blocks of cycles. Accordingly, the initial charging current was increased from 20 to 40% C_5 A after 250 cycles in the thin-plate test. A decline in capacity to 80% was found to follow an increase in voltage-limited return of charge, i.e. the recharge characteristics changed to that of a VRLA with a progressively lower degree of electrolyte saturation. In some instances, for diagnostic purposes, small amounts of acidified water were added to examine a possible influence on recharge response and available discharge capacity.

3. Results and discussion

3.1. Pre-matrix test—electrolyte saturation results

The 5-h rate capacities and ECE15L performance for the PNH, PNJ and PNK cells decrease with controlled reduction of the electrolyte saturation, see Table 7. The reduction in EV duty performance is 2 or 3% for 92% saturation, but increases to about 20% for 84% saturation. During the first 10 cycles, recharging was completed at a rate of 6% C_5A, after charge had been first returned to 80% state-of-charge at a current of 20% C_5. Cell-average states-of-charge at a polarization to 2.5 V are compared in Fig. 3 and Table 8 for the series PNH, PNJ, PNK. The recharge response appears to be strongly influenced by electrolyte/separator saturation. Polarization to gassing voltage is progressively delayed with increasing under-saturation. For the saturated

Table 7
Summary of measured performance of pre-matrix thin-plate cells

	PNH	PNJ	PNK
Saturation (%)	100	92	84
First average capacity at 14 A, 25 °C	78.1 Ah	72.6 Ah	70.7 Ah
Tenth average capacity at 14 A, 25 °C	77.5 Ah	72.7 Ah	70.9 Ah
String capacity at 14 A, 23 °C	74.0 Ah	72.1 Ah	67.4 Ah
ECE15L (string)	57.6 Ah	56.8 Ah	47.0 Ah
	654 Wh	642 Wh	523 Wh
String capacity at 14 A, 23 °C	71.2 Ah	69.9 Ah	67.7 Ah
ECE15L (string)	57.4 Ah	57.0 Ah	46.4 Ah
	652 Wh	641 Wh	514 Wh
String capacity at 14 A, 23 °C	71.0 Ah	68.9 Ah	67.5 Ah
ECE15L (string)	57.4 Ah	56.0 Ah	46.1 Ah
	652 Wh	630 Wh	510 Wh

Table 8
State-of-charge at polarization to 2.5 V per cell at 6% C_5 A

	PNH	PNJ	PNK
Separator saturation (%)	100	92	84
Cycle 2 recharge after measured discharge	97.7	106.0	111.2
Cycle 6 recharge after 75% discharge	98.3	101.8	105.0
Cycle 10 recharge after measured discharge	96.9	103.1	105.7

cell PNH, the voltage polarization anticipated return of charge is about 98%; charging will be voltage-limited before complete return of charge. When the separator saturation is in the range 90–95%, the voltage-limited overcharge amounts to 2–6% of nominal capacity at the expense of a performance loss of similar magnitude. At a lower saturation, the voltage-limited overcharge exceeds 5% C_5 and the capacity loss increases, i.e. to about 20% at 92% saturation. The capacity reduction penalty becomes unacceptable and the voltage-limited charge-acceptance is unnecessarily high. Following additional charge to complete the charging of negative plates, there is the possibility of the development of a high working temperature and thermal runaway with an electrolyte saturation of less than 90%.

For long cycle-life, charge algorithms should combine high coulombic efficiency, a low but sufficient charge factor, and a termination routine that is insensitive to any increase in the oxygen-recombination cycle rate associated with water loss.

At the expense of a reduction in discharge performance of 2 or 3% compared with a saturated cell, the initial target for saturation was set at 95% in order to achieve a balanced voltage-limited overcharge that would be stable throughout life with low overcharge charging. It was intended to match the chosen saturation with an IUI charging regime with approximately 2% C_5 overcharge within the 2.35 V per cell limited IUI phases and an overall overcharge as low as 4% C_5 per cycle.

3.2. 'Thin plate' matrix discharge performance test (11-plate design)

The results obtained from testing a string of six thin-plate cells are summarized in Table 9. The P-series cells, which have conventional positive active-material, exhibit stable performance. Cell performance is uniform within each group, and changes during characterization tests are small. The cells are limited by the performance of the positive plates and, hence, the influence of the separator and the negative plate variables are not significant in comparison with positive-plate cell variables. The 5-h discharge and specific energy for the ECE15L EV tests are enhanced for cells which have a high working concentration of electrolyte.

Stable performance is not, however, experienced during even the conditioning cycles for cells with positive active-material which has either a reduced mass or a lower density. For Q- and R-series cells, the density has been reduced, relative to the nominal process specification, by 7.5 and 15%, respectively. Following confirmation of poor ECE15L performance and diagnostic confirmation that performance
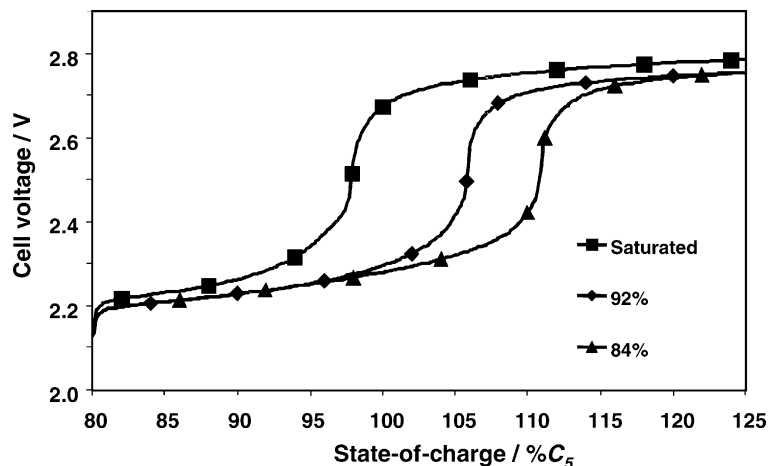

Fig. 3. Influence of oxygen-recombination rate on state-of-charge at 6% C_5 A.

Table 9
Results of test discharges for 11-plate (thin) design/process variables matrix

Cell	5-h at 25 °C		1st ECE15L		2nd ECE15L		3rd ECE15L		Average (Wh kg^{-1})	EUCAR 5 h at 23 °C			Discharges at 30 °C				
	1st	10th	Ah	Wh	Ah	Wh	Ah	Wh		1st	2nd	3rd	5 h	3 h	2 h	1 h	30 m
PNE-19	75.7	77.5	66.8	759	67.4	768	66.5	757	25.2	78.3	74.9	73.0	85.3	76.4	71.5	60.7	54.0
PNF-51	75.6	78.1	66.7	754	66.6	753	60.1	683	24.1	75.5	72.7	71.1	86.1	77.1	72.0	61.7	52.8
PNG-26	83.6	84.5	70.0	802	70.0	804	67.4	777	26.1	84.9	79.8	78.4	91.6	82.2	75.9	63.9	56.0
PME-71	82.8	81.0	66.8	761	66.5	757	66.6	761	25.5	84.2	73.1	79.3	83.8	78.2	72.4	62.3	53.6
PMF-74	80.4	79.2	66.6	755	65.7	745	66.3	756	25.3	79.4	75.5	76.9	80.6	75.5	69.1	59.5	50.8
PMG-83	86.1	82.2	66.8	756	66.7	768	66.3	759	25.6	84.4	79.5	78.7	82.7	74.9	69.0	60.4	51.7
PLE-G5	76.9	74.7	66.5	756	66.5	756	66.4	756	25.4	77.8	74.9	74.2	73.8	71.2	5.3	56.9	49.0
PLF-F3	74.4	75.1	65.8	747	65.8	746	65.6	745	25.0	76.7	73.4	72.7	76.2	70.5	65.4	57.3	49.1
PLG-H1	83.1	80.2	69.2	791	68.8	787	66.9	769	26.2	84.5	80.3	79.5	78.5	76.1	68.9	60.1	51.4
QNE-91	85.6	71.9	44.1	502	35.5	409	35.1	405	15.2	70.3	62.2	59.7	64.3	58.0	50.5	39.6	28.9
QNF-97	86.1	69.8	43.9	501	35.1	404	34.0	392	15.0	68.4	59.7	57.2	65.1	58.6	51.3	40.3	29.3
QNG-A4	94.5	73.5	44.3	422	26.0	247	16.4	155	11.4				49.9	42.7	32.2	21.7	15.7
QME-A9	83.9	69.7	44.3	505	37.6	429	34.9	403	15.7	74.5	63.8	62.0	74.6	65.9	56.5	44.0	32.8
QMF-B5	85.6	67.0	43.3	492	34.6	399	34.5	397	15.1	71.2	60.5	59.4	69.4	60.0	50.6	38.4	27.4
QMG-C1	96.4	79.3	44.3	516	43.3	495	34.3	400	16.5	79.0	65.2	62.3	63.1	52.9	43.6	31.7	22.3
RNE-C7	78.9	38.7															
RNF-D3	81.7	35.4					Early loss of capacity; no EV duty discharge test was made										
RNG-D91	90.4	36.6															

Positive plates: P, regular fill; Q, medium density; R: low density. Negative plates: N, regular over-pasting; M, flush pasting; L, low density, regular pasting. Separator and electrolyte variants: E, normal plate wrap, 1.300 rel. dens; F, positive plate wrap, 1.300 rel. dens; G, normal plate wrap, 1.320 rel. dens.

is limited by polarization of the positive plates, testing of other cells using such plates was suspended. There are some examples of enhanced initial performance with low-density material, but the capacity declines during 10 cycles and sometimes even the initial performance is not improved.

The best *thin-plate* cell performance is achieved with P-series cells, the 'nominal' design. The performance is enhanced by increasing the relative density of the electrolyte by 0.020 in cell PNG. The projected performance with this 11-plate cell in a six-cell monobloc is presented in Table 10. The performance is good with an ECE15L specific energy that is 44% greater than that achieved with existing tubular technology, and is within the spread of values reported for pasted-plate VRLA batteries.

Table 10
Specific energy of thin-plate (11 plate) PNG cells

				5-h rate at 30 °C		ECE15L 804 Wh (g Wh^{-1})
				91.6 Ah (g Ah^{-1})	1083 Wh (g Wh^{-1})	
		Component mass (g)				
Container and lid			1775	3	2	2
Pillars			170	0	0	0
Intercell connectors			1100	2	1	1
Burning strip			480	1	0	1
AGM			588	1	1	1
Positive plates			11543	21	11	14
Negative plates			8205	15	8	10
Electrolyte			6600	12	6	8
	Each	Number	Per battery			
Spine	125	30	3750	7	3	5
Gauntlet	13.9	30	417	1	0	1
Bottom bar	2.5	30	75	0	0	0
PAM			7301	13	7	9
Neg grid	74.7	36	2689.2	5	2	3
NAM			5515.8	10	5	7
Top lead			1750	3	2	2
Battery mass			30461	55	28	38
Battery (Wh kg^{-1})					36	26

Table 11
Results of test discharges for 13-plate (thinner) design/process variables matrix

Cell	5-h at 25 °C		1st ECE15L		2nd ECE15L		3rd ECE15L		Average (Wh kg^{-1})	EUCAR 5-h at 23 °C			Discharges at 30 °C				
	1st	10th	Ah	Wh	Ah	Wh	Ah	Wh		1st	2nd	3rd	5 h	3 h	2 h	1 h	30 m
SNE-19	81.2	83.8	77.1	883	70.5	810	68.3	788	26.9	83.9	79.4	78.0	80.2	75.0	70.6	63.1	55.0
SNF-25	89.5	86.5	77.2	884	70.8	813	68.2	786	27.0	87.1	81.6	79.3	83.9	74.8	68.8	60.1	49.1
SNG-31	88.9	88.2	78.0	902	77.7	900	77.4	898	29.2	87.3	84.0	83.6	84.7	78.7	75.2	65.8	57.2
SLE-D2	87.3	85.2	67.8	780	67.2	773	66.3	761	25.4	82.7	76.8	75.6	78.1	71.7	66.0	56.9	47.9
SLF-D8	90.3	88.7	76.5	876	67.5	778	67.1	772	26.6	88.5	81.2	78.2	77.5	69.5	65.4	54.8	45.4
SLG-E1	94.7	91.4	76.9	890	69.4	806	67.3	783	27.1	76.9	69.4	67.3	80.4	72.6	66.3	56.9	47.8
TNE-37	92.7	72.1	44.8	519	36.1	420	35.1	408	15.0	61.1	50.4	46.2	44.2	38.2	30.9	22.6	16.5
TNF-43	77.3	55.9	38.5	446	33.5	387	34.8	404	13.8	62.3	44.6	43.4	58.8	49.3	40.4	29.4	19.7
TNG-49	72.9	55.3					Early loss of capacity; no EV duty discharge test was made										
UNE-67	54.3	22.8					Early loss of capacity; no EV duty discharge test was made										

Positive plates: S, regular fill; T, medium density; U, low density. Negative plates: N, regular over-pasting; L, low density, regular pasting. Separator and electrolyte variants: E, normal plate wrap, 1.300 rel. dens; F, positive plate wrap, 1.300 rel. dens; G: normal plate wrap, 1.320 rel. dens.

3.3. Thinner-plate matrix test (13-plate design)

The performance of thinner-plate cells in a six-cell string is summarized in Table 11. The performance of the S-series of cells is stable, but is relatively insensitive to controlled variables other than an improvement in capacity and specific energy for the variable *G* which uses acid of high relative density. As with the thin-plate design, poor performance is experienced with T- and U-series cells which contain positive plates with reduced positive active-material density and mass. Poor and declining performance is confirmed for tests according to ECE15L, and half-cell measurements show that positive-plate polarization is the limiting determinant of discharge performance.

The discharge performance on the second and tenth cycles of SNE cells and SNG cells with higher acid relative density is shown in Fig. 4. The discharge capacities of positive plates filled according to the normal specification do not decline with cycling. There is no strong polarization at the start of recharge following the measured discharges. For cells with
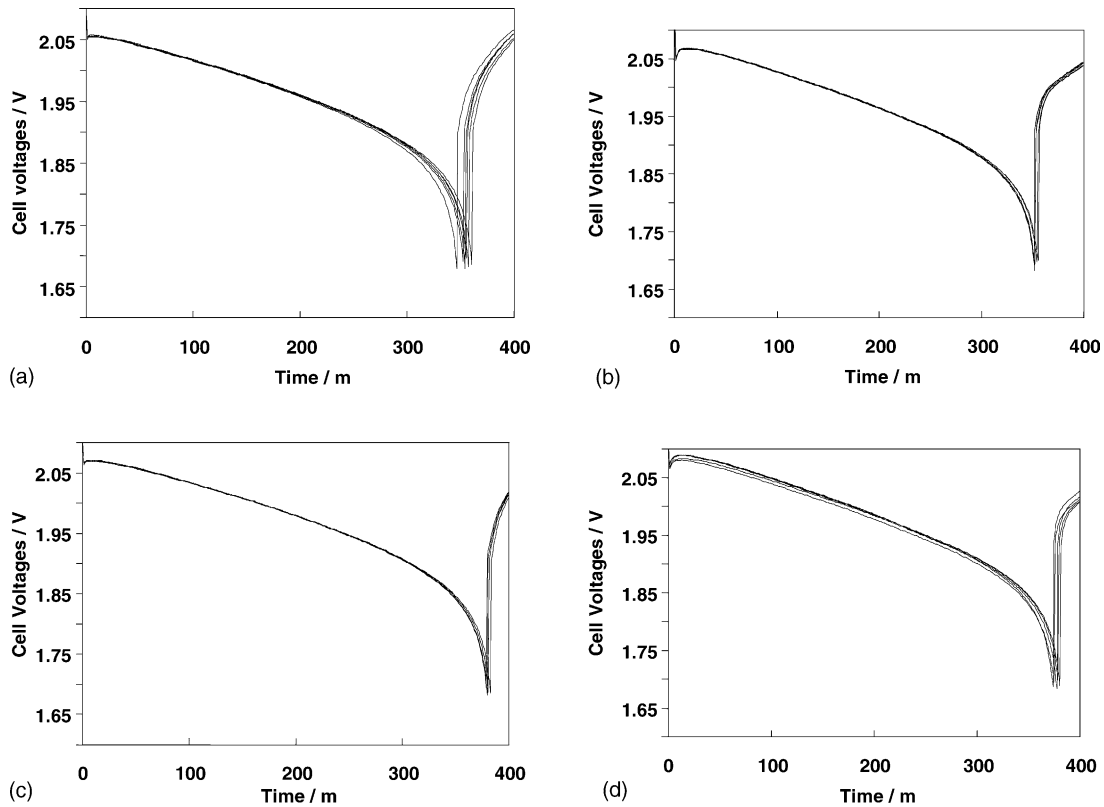

Fig. 4. Constant-current discharge curves (5-h rate) for thinner-plate cells. SNE cells after (a) 2 cycles, (b) 10 cycles. SNG cells after (c) 2 cycles, (d) 10 cycles.

Table 12
Specific energy of thinner-plate (13 plate) SNG cells

| | Each | Number | Per battery | 5-h rate at 30 °C | | ECE15L |
				85.0 Ah (g Ah^{-1})	1003 Wh (g Wh^{-1})	900 Wh (g Wh^{-1})
		Component mass (g)				
Container and lid			1775	3	2	2
Pillars			170	0	0	0
Intercell connectors			1100	2	1	1
Burning strip			480	1	0	1
AGM			541	1	1	1
Positive plates			11575	23	12	13
Negative plates			8660	17	9	10
Electrolyte			6450	13	6	7
Spine	127.7	36	4597.2	9	5	5
Gauntlet	13.4	36	482.4	1	0	1
Bottom bar	2.4	36	86.4	0	0	0
PAM			6409	13	6	7
Neg grid	61.5	42	2583	5	3	3
NAM			6077	12	6	7
Top lead			1750	3	2	2
Battery mass			30751	60	31	34
Battery (Wh kg^{-1})					33	29

reduced positive active-material density, discharge on the tenth cycle is shorter than that on the second cycle and recharge voltages are increased at the start of recharge.

The best thinner-plate performance is achieved with the 'nominal' design. The performance is enhanced by increasing the relative density of the acid by 0.020 in variant SNG. The projected performance of this 13-plate cell in a six-cell monobloc is presented in Table 12. The ECE15L specific energy is 10% greater than the excellent result obtained above for the thin-plate design and 60% greater than that for existing tubular-plate technology.

The enhancement of ECE15L performance is illustrated for the evolving plate design in Fig. 5. Voltage and current discharge curves are presented for strings of cells based on existing technology (Fig. 5(a)), using 5.25-mm thick plates, and for the two development designs (Fig. 5(b) and (c)).

3.4. Design review

The thinner-plate design demonstrates the benefit of the additional plate couple for high-rate performance in ECE15L EV tests. The enhanced performance associated with increased acid relative density may prove to be at the expense of life; two levels are adopted as controlled variables for the cycle-life testing phase.

Decrease in the amount of positive active-material gives unsatisfactory results. Though possibly not significant, cells with material in the convention range of density appear to give better specific energy when using positive plates of higher weight.

Although half-cell measurements indicate only a minor contribution from the polarization of negative plates, reduc-

tion in the amount of negative active-material by using thinner plates or lower density plates and increasing the electrolyte quantity according to the reduction in negative active-material volume, fails to raise the specific energy of the cells. Given frequent reports of negative-plate limitation of VRLA battery life, the 'nominal' design of negative plate was retained without precluding future attempts to exploit the apparent reserve of negative-plate performance.

Using a positive-plate separator wrap may enhance the uniformity of electrolyte availability to outboard positive plates, but this would be at the expense of marginally increasing the plate pitch. As this variant does not control cell performance, a conventional plate wrap is used to elevate the negative plate and improve the vertical alignment of positive and negative active-materials.

3.5. 'Thin-plate' cycle test results

In cycle testing of both thin- and thinner-plate cells, where actual discharge amounted to 80% of nominal capacity, the end-of-discharge voltage (EoDV) was used as an indication of available capacity. The EoDV at 80% DoD was about 1.90 V when available capacity was 100% and fell to 1.70 V when the capacity had fallen to 80%.

3.5.1. Cycle testing thin-plate cell PME71 with IUI charging to +4%, +6% C_5 and PSoC

On cycling to 80% DoD with IUI charging to +4% C_5, the available capacity of the thin-plate cells fell to 80% in 40 cycles (see Fig. 6), but recovered during cycles 51–100 for which the overcharge per cycle was increased to 6% C_5. The end-of-discharge voltage at 80% DoD increases following

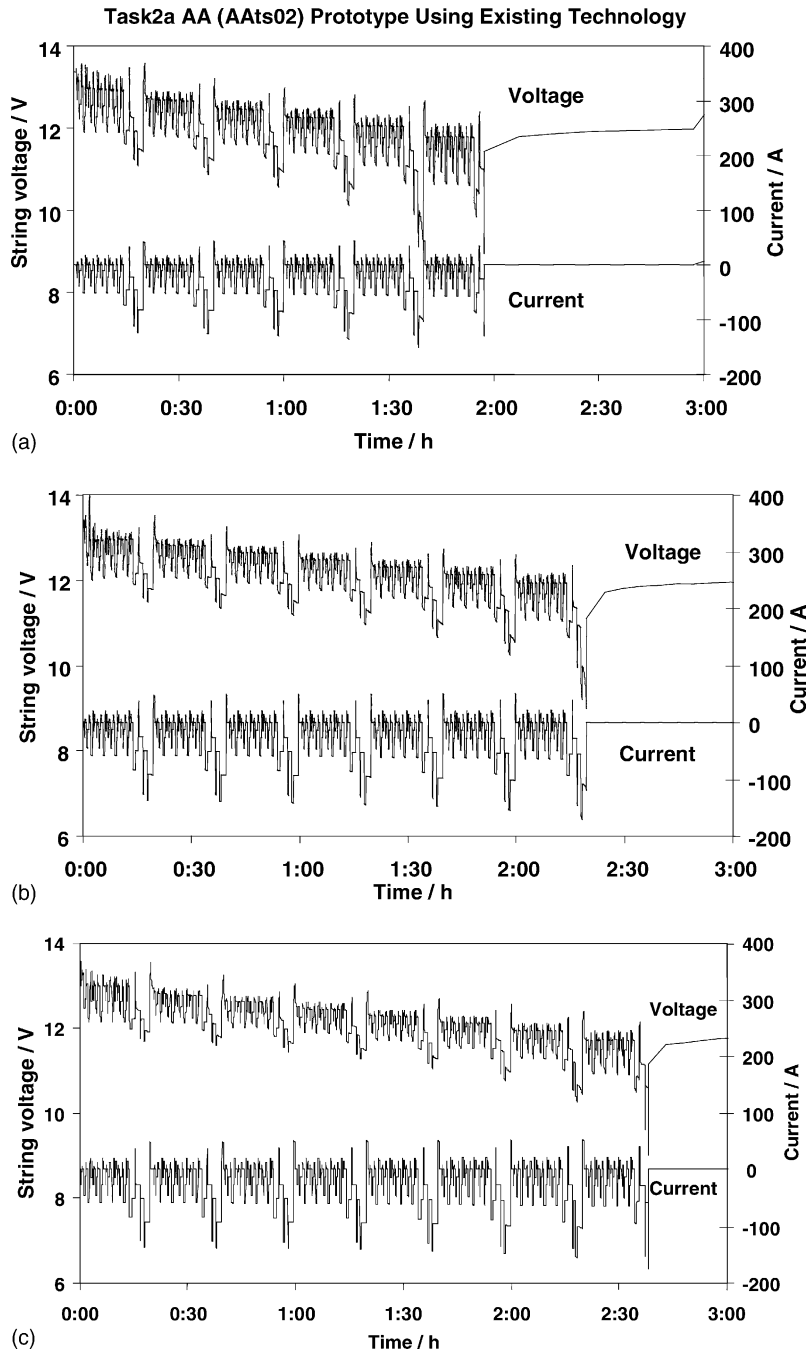**Task2a AA (AAts02) Prototype Using Existing Technology**

(a)

(b)

(c)

Fig. 5. Progressive enhancement of ECE15L performance with change in cell design: (a) conventional technology; (b) thin-plate cell; (c) thinner-plate cell.

the break between 50 cycle blocks. When PSoC operation, with two cycles of IU charging and one IUI to 6% C_5, was applied during cycles 101–150, the end-of-discharge voltage fell more rapidly. Data points are at 5-cycle intervals so, for that interval, the data reflect the situation for recharge to the voltage limit or recharge with 6% overcharge for that cycle.

From cycle 200, with IUI charging to +6% C_5, the EoDV declined during blocks of successive cycles and recovered during the intervals between blocks. From cycle 251, the initial charging current was increased to 40% C_5 A and the rate of fall of the EoDV was diminished for successive

cycles. Reflecting available capacity, this voltage pattern continued until the capacity fell below 80% after 610 cycles. During 550 cycles, the voltage-limited (2.35 V) return of charge increased from 1.4 to 3.4% C_5 and the cell voltage rose to over 2.6 V at the end of every IUI recharge.

A small electrolyte restoration after 550 cycles may have been followed by an improvement of performance but erratic recharge voltages after cycle 600 probably indicate the development of an intermittent internal short-circuit. The pattern of declining and recovering capacity continued until testing was terminated after 750 cycles.
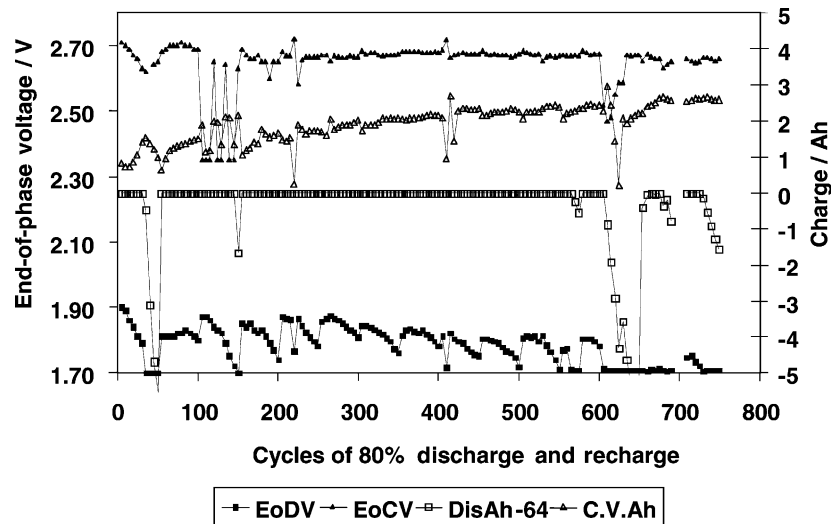
Fig. 6. Cycle test results for thin-plate cell PME71. EoDV: end-of-discharge voltage; EoCV: end-of-charge voltage at 1.6% C_5 A; DisAh-64: discharge capacity, relative to 64 Ah, the nominal 80% discharge (a point at -1.0 Ah indicates that discharge is voltage limited at 63 Ah); C.V.Ah: return of charge at end of U, net of discharge.

3.5.2. Cycle testing thin-plate cell PME72 with IUI charging to +6% C_5

On cycling to 80% DoD with IUI charging to +6% C_5, the available capacity of the thin-plate cells fell, and then recovered, during the first 50 cycles as indicated by the EoDV in Fig. 7. The EoDV declined during blocks of successive cycles and recovered during the intervals between blocks. Like cell PME71, from cycle 251, the initial charging current from increased 20% C_5 A to 40% C_5 A; the rate of fall of the EoDV was diminished for successive cycles; the capacity fell to less than 80% after 530 cycles. After a small restoration of electrolyte at cycle 550, and without additional charge, the performance recovered and still exceeded 80% at cycle 750. During 550 cycles, the

voltage-limited (2.35 V) return of charge increased rapidly from 0 to +1.5 C_5 during the first 50 cycles, and then to +4.0% C_5. The cell voltage increased to over 2.6 V at the end of every recharge.

3.5.3. 'Thin-plate' cycle test discussion

The rate of decline in the EoDV does not decrease during cycles 100–150 under partial-state-of-charge operation. For charging with a low charge factor, partial-state-of-charge operation is not beneficial.

The capacities of the cells decline with successive cycles and recover between blocks. This characteristic is attributed to the high gamma of the design and is barely perceptible in tests with the thinner-plate design which has a low value of
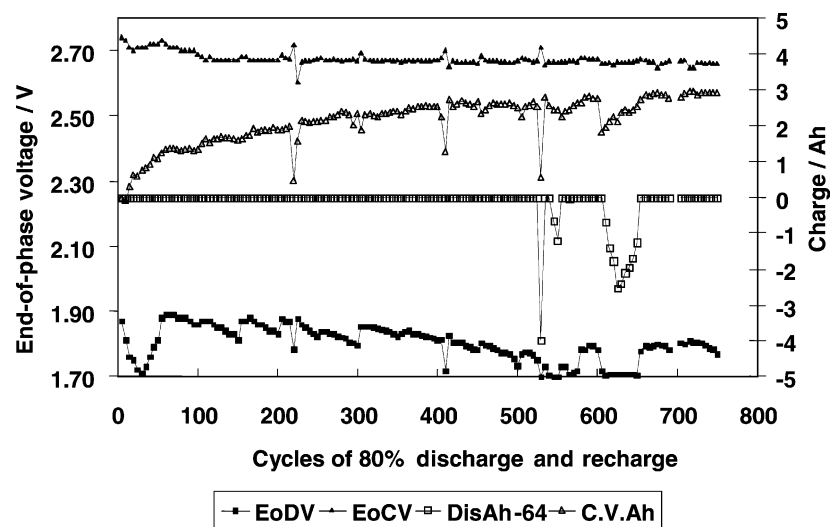

Fig. 7. Cycle test results for thin-plate cell PME72. EoDV: end-of-discharge voltage; EoCV: end-of-charge voltage at 1.6% C_5 A; DisAh-64: discharge capacity, relative to 64 Ah, the nominal 80% discharge (a point at -1.0 Ah indicates that discharge is voltage limited at 63 Ah); C.V.Ah: return of charge at end of U, net of discharge.

gamma. This characteristic is mitigated when the initial charge rate is increased after 250 cycles.

Reversible loss of available capacity is observed in cells where the design reduction of spine metal results in a gamma of $1.2\,\mathrm{g\,cm^{-2}}$, but not by the thinner-plate cells where Pavlov's recommendation of $0.8\,\mathrm{g\,cm^{-2}}$ [1] has been applied. The performance was sustained with 6% C_5 overcharge, but not with the 4% C_5 that is sufficient for the thinner-plate design. This behaviour is probably related to the thickness of the positive active-material.

Although maintenance of performance was poor in comparison with the thinner-plate cells, oxygen cycle was sufficient to obtain balanced recharge of the positive and negative plates at about 2.5% C_5 overcharge and polarization to gassing voltage during further overcharge at a low rate of charge was sustained for a large number of cycles.

3.6. 'Thinner-plate' cycle test results

3.6.1. Cycle testing thinner-plate cell SNE13 with IUI charging to +4% C_5

The cycle-life of cell SNE13 at 80% DoD with IUI charging (20% C_5 A, 2.35 V, 1.6% C_5 A to +4% C_5 overcharge per cycle) is shown in Fig. 8. It is seen that the cell maintained a capacity that was greater than 80% for 1050 cycles. As an indicator of available capacity, the EoDV declined only slowly for 900 cycles, and then dropped at an increasing rate to 80% at 1050 cycles. The capacity was greater than 75% when testing was stopped at 1100 cycles. The voltage-limited return of charge increased from +1.1 to +1.8% C_5 during the first 50 cycles and then to +3% C_5 after 110 cycles. The cell voltage rose to over 2.6 V for a short period at the end of every cycle. Development of the recharge response of the cell during life is discussed below in Section 3.7. The indication from other tests that

performance might be restored by a small addition of electrolyte was not tested.

3.6.2. Cycle-testing thinner-plate cell SNE14 with IUI charging to +6%, PSoC and 4% C_5

Testing of cell SNE14 at 80% DoD with IUI charging (20% C_5 A, 2.35 V, 1.6% C_5 A) initially to 6% C_5 overcharge per cycle was changed to PSoC operation from cycles 101–600, Fig. 9. Charging was terminated at the end of the constant-voltage phase for two IUI cycles and then IUI charging to +6% C_5 was applied on the third cycle. During PSoC operation, the EoDV increasingly varied according to the number of cycles since the last complete recharge. A higher EoDV following complete recharge is taken to reflect a higher available capacity than the lower EoDV that followed limited recharge. As indicated by the 80% EoDV, the available capacity declined slowly to 80% following incomplete recharge after 550 cycles and after 600 cycles for the discharge that followed the occasional IUI charging. The capacity did not recover with IUI charging to +4% C_5 every cycle or following extra charge during cycles 600–650. Return of charge at the end of the controlled voltage stage (EoCV) was a little high, compared with cell SNE13. As this suggested a modest reduction in saturation, 30 ml of dilute electrolyte (relative to 1 kg electrolyte) was added to investigate the impact on the oxygen-recombination controlled recharge at cycle 650. The voltage-limited return of charge fell to that shown by SNE13 initially and, without additional charge, the capacity recovered within a small number of IUI, +4% C_5 cycles. This treatment was repeated after a further 150 cycles when the capacity had again fallen to 80% after 900 cycles. Again, a recovery in capacity was observed.

With 6% C_5 overcharge per cycle, the voltage-limited return of charge increased rapidly from +2.1 to +3.4% C_5 during the first 100 cycles. For PSoC operation between
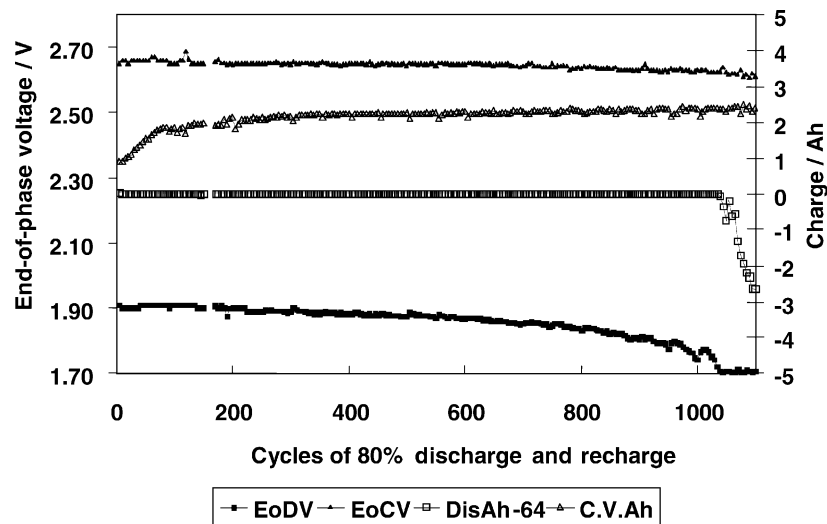

Fig. 8. Cycle test results for thinner-plate cell SNE13 with IUI charging to +4% C_5. EoDV: end-of-discharge voltage; EoCV: end-of-charge voltage at 1.6% C_5 A; DisAh-64: discharge capacity, relative to 64 Ah, the nominal 80% discharge (a point at −1.0 Ah indicates that discharge is voltage limited at 63 Ah); C.V.Ah: return of charge at end of U, net of discharge.
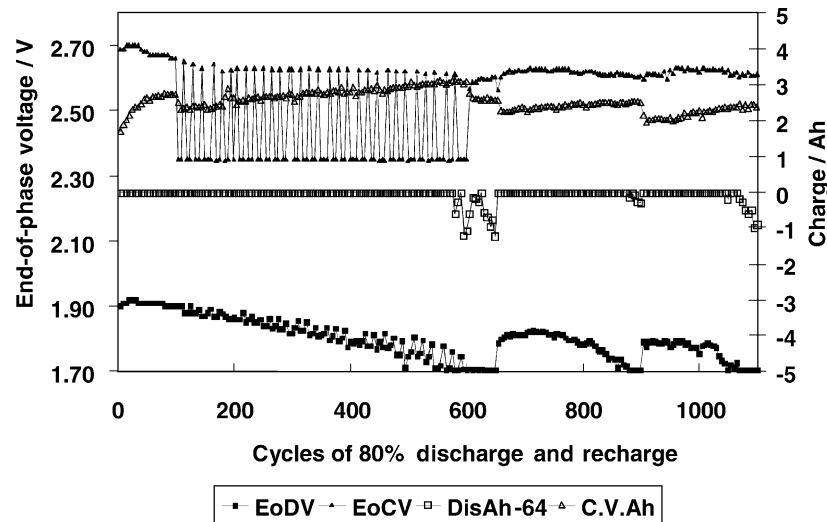
Fig. 9. Cycle tests results for thinner-plate cell SNE14. EoDV: end-of-discharge voltage; EoCV: end-of-charge voltage at 1.6% C_5 A; DisAh-64: discharge capacity, relative to 64 Ah, the nominal 80% discharge (a point at -1.0 Ah indicates that discharge is voltage limited at 63 Ah); C.V.Ah: return of charge at end of U, net of discharge.

cycles 101 and 600, the voltage-limited return of charge increased from $+2.9$ to $+3.8\%$ C_5 overcharge per cycle and stabilized at $+3.2\%$ C_5 for IUI charging to $+4\%$ C_5. Reflecting the oxygen-recombination rate and its dependence on water loss and electrolyte saturation, the voltage-limited return of charge fell from $+3.2$ to $+2.8\%$ C_5 on the first addition of electrolyte was made after 650 cycles, and from $+3.1$ to $+2.5\%$ C_5 on the second addition at 900 cycles. The available capacity was 79% of nominal when cycle testing was stopped at 1150 cycles.

3.6.3. Thinner-plate end-of-cycle test examination

Cells SNE13 and SNE14 were dismantled and examined for defects and signs of component deterioration. Except for dull material at the bottoms of the plates, the negative material appeared to be in good condition and gave a metallic smear over most of the area. All components appeared to be in good condition. Positive spine corrosion was moderate; the spines had remained robust and intact. The bottom bars of the positive plates were loose and this possibly indicates slight spine growth (i.e. to less than 1 mm). Photographs of cycled positive plates from cells SNE13 and SNE14 are shown in Fig. 10, respectively. There was no indication of active-material shedding in either plate.

The AGM separator was split to represent three equal height zones for representative determination of wet mass and electrolyte relative density. Samples of positive and negative active-materials were also taken for lead sulfate analysis. The results of these analyses are presented in Table 13. There is no marked variation in separator saturation with height. Low stratification is demonstrated by the small variation of electrolyte concentration with height. Analysis of lead sulfate indicates that much of the active-material is in a reasonable state-of-charge. Sulfation of the
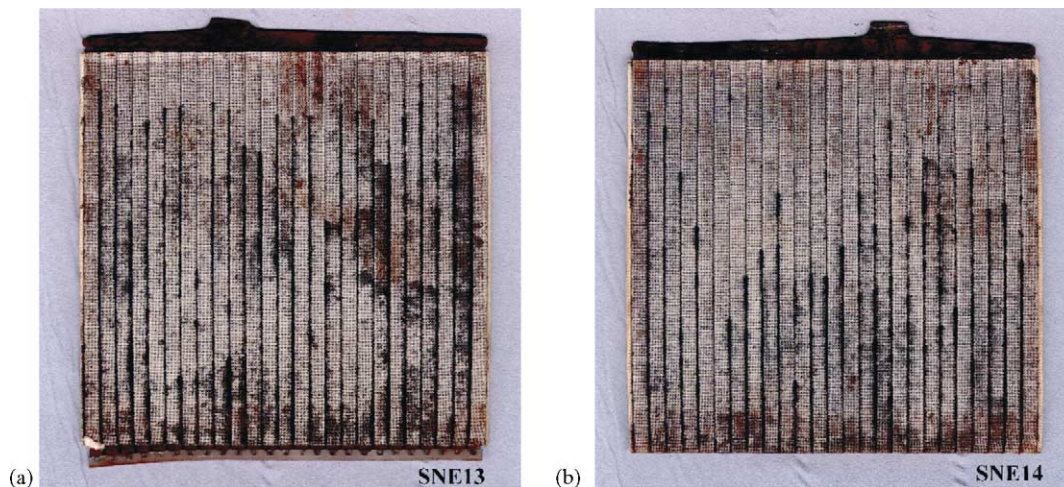

Fig. 10. Photographs of positive plate at end of life from (a) cell SNE13 and (b) cell SNE14.

Table 13
Electrolyte and lead sulfate distribution at the end-of-life

	Wet AGM mass	Acid rel. dens in AGM	$PbSO_4$ (wt.%) in positive	$PbSO_4$ (wt.%) in negative
SNE13 examination after 1100 cycles				
Top	172.1	1.290	6.8	2.5
Middle	162.9	1.310	9.2	1.0
Bottom	161.3	1.315	8.6	17.1
SNE14 examination after 1150 cycles				
Top	165.2	1.252	6.0	2.2
Middle	158.3	1.289	5.2	2.5
Bottom	150.4	1.300	15.3	63.5

active-material at the bottom of the plates is, however, sufficient to deplete the electrolyte concentration such that it influences positive-plate performance. Except at the bottom of the plates, the negative material from cells SNE13 and SNE14 has a high state-of-charge.

Sections of a spine at the end of cell life are illustrated in Fig. 11(c)–(f), together with reference samples from an un-cycled battery MA10 in Fig. 11(a) and (b). Two sections are presented for each test cell. With a lower magnification and a 3.1 mm × 2.4 mm field of view, one image illustrates the whole section for comparison of the extent of corrosion, and the other image (with a 1.2 mm × 0.9 mm field of view)
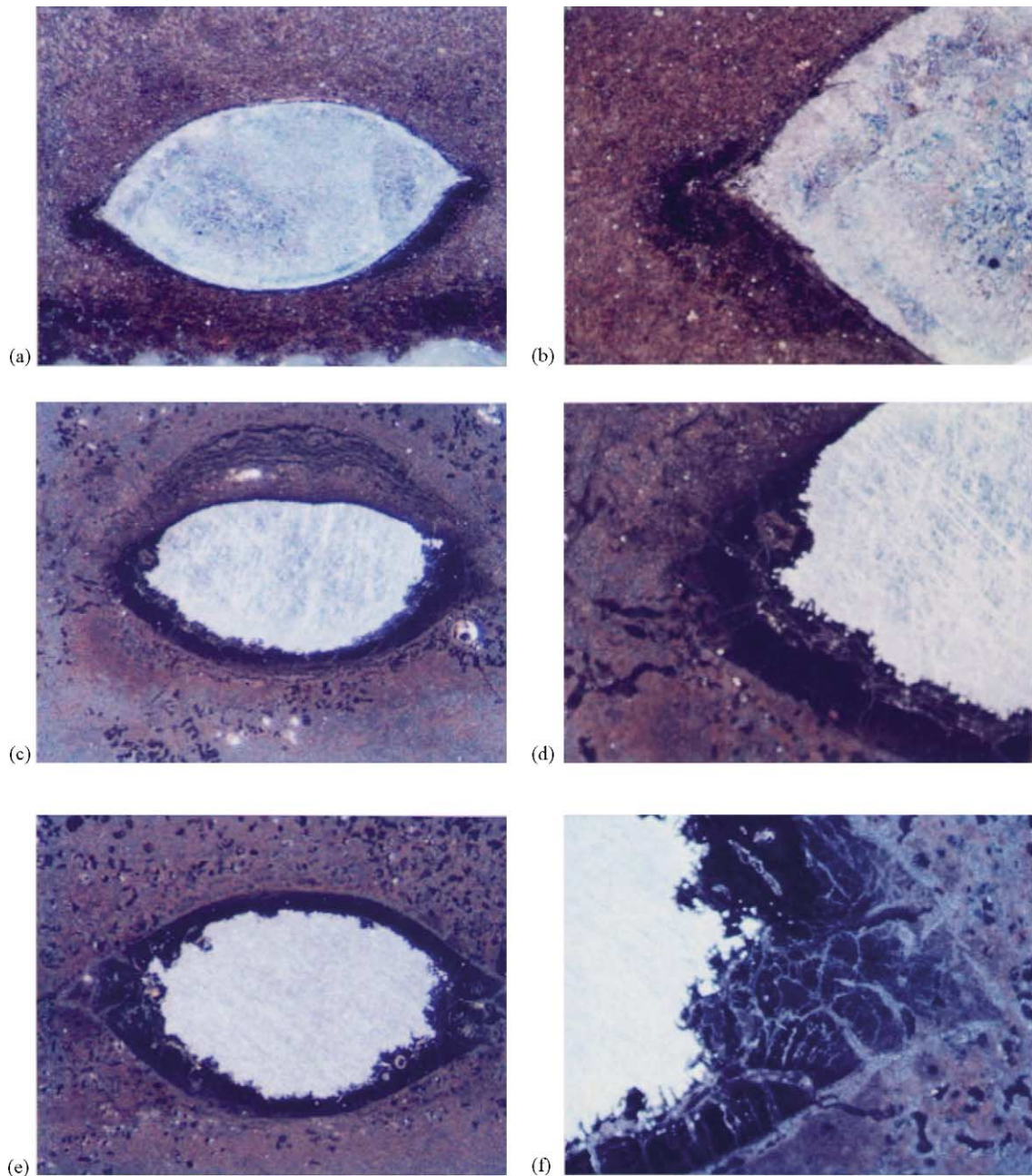

Fig. 11. Photographs of spine sections from: (a) and (b) un-cycled battery MA10; (c) and (d) cell SNE13 after 1150 cycles to 80% DoD; (e) and (f) cell SNE14 after 1150 cycles to 80% DoD.

shows the relatively small extent of penetrating corrosion at higher magnification. The residual cross-sectional area is 63 and 68% for cells SNE13 and SNE14, respectively. Both cells experienced an average corrosion depth of 0.012 mm.

3.6.4. 'Thinner-plate' cycle test discussion

Excellent cycle-life was achieved with low overcharge charging of thinner-plate cells that had an initial saturation designed to achieve a balanced and sufficient charge within a low voltage limit. With low charge factor, however, PSoC operation was not beneficial.

Improvement in charge efficiency or cycle performance, relative to the thin-plate design, may arise from the lower gamma value of the thinner-plate design, as well as the lower 'geometric' current density and the reduced thickness of the positive active-material. Results obtained to date encourage further development of the thinner-plate design. With a gamma of $0.85 \, \text{g cm}^{-2}$, thinner-plate cells do not exhibit capacity loss that is premature or reversible. After 1100 cycles, the cell components are still healthy. Rather, endurance is limited by water loss from the electrolyte and the consequent decline in the state-of-charge of the negative active-material.

3.7. Saturation, oxygen cycle and balanced charge factor

For cells with different controlled electrolyte saturations, polarization towards the end-of-charge is illustrated in Fig. 3. In the test applied, recharge was at a constant current of 6% C_5 A after recharging to 80% state-of-charge at 20% C_5 A. For the electrolyte-saturated cell PNH, polarization towards the end-of-charge accelerated as recharge approached the discharge capacity with an apparent state-of-charge which amounted to 98%. The rapid increase in cell voltage is attributed to a change from charge-acceptance by the negative active-material, with a relatively low overpotential, to hydrogen evolution, with a higher overpotential, as the conversion of lead sulfate to lead approaches completion.

As described by Peters et al. [6], the charge efficiency of the positive active-material declines at a lower state-of-charge than does that of the negative active-material. Thus, the transition to oxygen evolution at the positive plate is more gradual than the transition from charge-acceptance to hydrogen evolution at the negative plate. Depending on recharge rate and temperature, the charge-acceptance of positive active-material may start to fall when the state-of-charge is less than 80% and the balance of charge reaches completion after 100% return of charge. Oxygen is produced at the positive plate as the charge-acceptance falls, both before 100% return of charge and before the charge-acceptance of the negative plate declines.

As saturation is reduced in cells PNJ and PNK, there is a strong influence of oxygen-recombination in delaying the cell polarization associated with the onset of hydrogen evolution. Lower saturation of the separators facilitates the transport of oxygen from the positive to the negative

plate where it reacts with the active-material. Oxidation of the negative active-material equates to a reduction in its state-of-charge.

In cycling applications, oxygen-recombination delays the recharge of the negative plates. This offers the potential, through controlling saturation and oxygen-recombination rate, to compensate for the lower charge efficiency of positive plates by delaying the full recharge of the negative plates so that both approach full charge together and with modest overcharge. For example, positive plates that require 4% C_5 overcharge per cycle may suffer from undercharging in a saturated electrolyte cell where voltage-controlled charging becomes limited after 98% return of charge. With the lowest level of saturation (viz. 84%), cell PNK does not polarize until the overcharge is more than 5% C_5. Here, the increase in the potential of the negative plate is delayed by the higher rate of oxygen-recombination to the extent that when charging becomes voltage limited, the overcharge requirement of the positive plates has been exceeded and further overcharge is still necessary to complete the charging of the negative plates. At about 95% saturation, balanced charging can be achieved for IUI charging when the negative-plate polarization is delayed to about 2% C_5 overcharge and total overcharge amounts to 4% C_5. This also shows how a small change in the cell condition can result in a large change in the recharge from a charger with control features that are responsive to cell voltage. Even with an optimized design, if walk-down due to undercharging is to be avoided, there is a slow reduction in saturation as water is lost.

The change in the response of an initially 95% saturated cell with water loss during life is shown in Fig. 8. On cycling with an IUI characteristic and 4% C_5 overcharge every cycle, the 80% EoDV declines during 1050 cycles. The C.V.Ah curve is the balance of charge at the end of the constant-voltage phase of charge. The voltage-limited return of charge is increased most strongly in early cycles as the oxygen-recombination rate increases. After 100 cycles, the continuing increase is slow. The EoCV curve is the low-rate end-of-charge voltage. Cell voltage continues to polarize to the gassing voltage for a short and declining period at the end-of-charge throughout the test.

The change in the voltage and voltage-limited current, in relation to return of charge, during the first 900 cycles of the test is given in Fig. 12. The voltage curves are identified by the legends with the letter 'V' followed by the cycle number, and the charging current curves by the letter 'I' followed by the cycle number. For example, V 15 is the charge voltage curve for cycle 15, and I 250 is the current curve for cycle 250. IUI charging was conducted at 20% C_5 A to 2.35 V, at 2.35 V until the current declined to 1.6% C_5 A and continued at that rate until 4% overcharge. Due to an increasing oxygen-recombination rate during recharge, polarization of the negative plates was delayed increasingly on progressive cycles. The changes are relatively large between the square-marked curves at 15 cycles, the diamond-marked curves at 50 cycles and the triangle-marked curves at 250
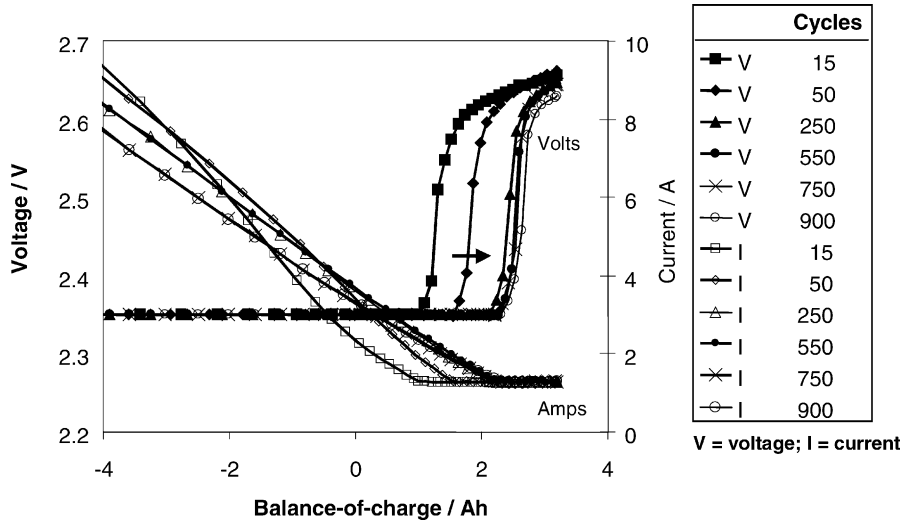
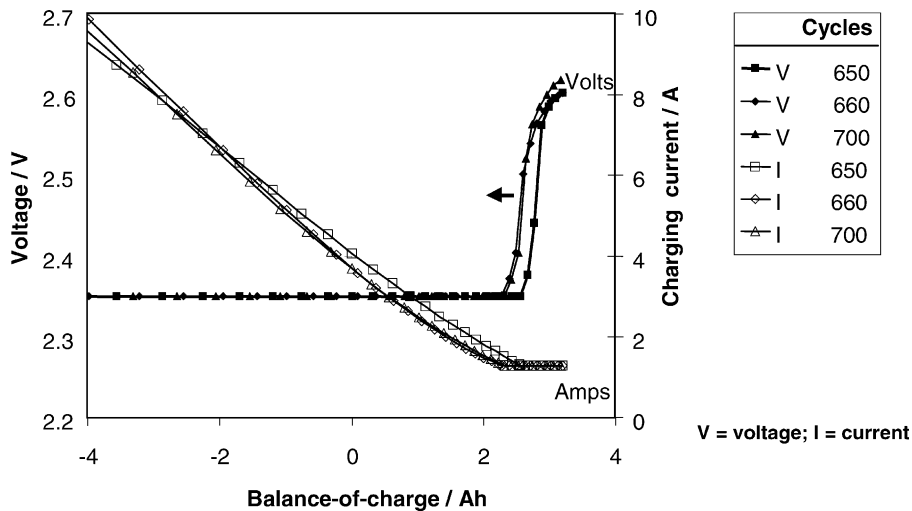Fig. 12. Delayed negative-plate polarization as water is lost during the cycle-life of cell SNE13.

Fig. 13. Earlier polarization following restoration of depleted electrolyte to cell SNE14.

cycles. Subsequent changes, up to 900 cycles, are relatively small.

The decline in the EODV for a similar cell SNE14 operating with different charging conditions is shown in Fig. 9. In that test, the EoDV declined to 1.7 V during 550 cycles and did not recover with the more favourable charge regime used for the test used for the data in Fig. 9 or following additional charge. The performance did, however, recover with continued IUI 4% overcharge cycling after a small (30 g in 1 kg of electrolyte) restoration to the electrolyte.

The change in charge response of the cell after the small addition of water during cycle 661 is shown in Fig. 13. The capacity increases from 78 to 80% by cycle 670, after which the EoDV continues to increase. The polarization at the end-of-charge, that had been delayed in relation to state-of-charge as saturation declined during life, reverted after the small addition of water.

For long cycle-life, charge algorithms should combine high coulombic efficiency, a low but sufficient charge factor, and a termination routine that is insensitive to any increase in oxygen-recombination rate associated with water loss. Controlling the initial saturation to about 95% stabilizes the response to charge, as saturation declines during life through water loss. A charge characteristic that is appropriate for 95% charging would undercharge a saturated cell; a charge regime that would recharge a saturated cell would overcharge and accelerate the drying-out process after saturation is reduced during early cycles.

4. Conclusions

A design strategy for improving the performance of tubular-plate batteries under EV duty by reducing plate thickness and increasing the number of plate couples within

a fixed cell length has been successfully implemented. Enhanced performance is sustained when decrease in the amount of inactive metal is limited to that available through adopting an elliptical spine section to maintain the contact area between the spine and the positive active-material. Substantially thinner spines and plates have been satisfactorily processed in manufactured quantities. Thinner plates improve performance and charge-acceptance, particularly at higher rates. Good cycle-life of positive and negative plates is achieved with optimized cell design and appropriate charging with low overcharge.

4.1. Performance achievements

Based on the measured performance of test cells and the battery design component masses of the thin plate design, an ECE15L specific energy of 26 Wh kg^{-1} equates to a 44% improvement on expectations based on tests of model cells with existing commercial tubular-plate designs. With an additional extra couple in the same container, the thinner-plate design increases the specific energy to 29 Wh kg^{-1}. This is a 60% enhancement of what can be expected from existing technology. With designs optimized for the EV duty, specific energies at the 5-h rate of discharge are 36 and 33 Wh kg^{-1} for the thin-plate and thinner-plate designs.

4.2. Cycle-life achievements

Cycling at $C_5/5$ A to 80% of peak achieved capacity and the best charge regime (IUI to +4% C_5), the available capacity exceeds 80% of nominal for 1050 cycles. Performance loss is due to water loss from the electrolyte; plates are in good condition at the end of life. Earlier loss of capacity after cycling with different charging conditions can be reversed by a small addition of acidified water and continued cycling with the preferred charging method.

4.3. Charge-acceptance/efficiency

In an associated project [7], the improved charge-acceptance of the thinner-plate cells has been reported in the context of fast charging. It has been established that the capacity of thinner-plate cells is sustained with only 4% C_5 overcharge per cycle; the capacity of thin-plate cells declines during cycles with 4% C_5 overcharge per cycle but is sustained by 6% C_5 overcharge per cycle. The apparent difference in favour of the thinner plates may be exacerbated by the high gamma value of the thin-plate design which results in reversible decline in discharge performance for successive cycles.

4.4. Designed stabilization of oxygen cycle for charging

The cell design is optimized for oxygen-recombination to delay negative-plate recharge sufficiently to have both positive and negative plates approach full recharge together with low overcharge. An appropriate, low overcharge, recharging regime gives stable operating conditions over a long cycle-life. Negative plate health is maintained by a short period of polarization included at the end of every recharge. The charging characteristics change slightly as water is lost, and this delays and shortens the period of negative-plate polarization. Delayed polarization and reduction of discharge capacity that are associated with water loss from the electrolyte can both be reversed, by small restoration of water and continued charging with a low charge factor.

4.5. Reduction of positive active-material density

It was expected that decrease in the density of the positive active-material would improve cell performance by enhancing the supply of electrolyte within the plates. Testing two levels of density below that optimized for existing products failed, however, to improve the specific energy of the cells because available capacity deteriorated with cycling.

4.6. Metal saving and gamma

It is possible to increase the specific energy by reducing the amount of the inactive material that serves as an electronic conductor to the plates. The lead-alloy spines of tubular positive plates that have to fulfil a mechanical-supporting role are diminished and weakened during life by corrosion; available discharge performance may be impaired if the gamma value of the active mass to the conductor surface area is too high.

By using an elliptical spine section instead of one that is almost circular, the spine mass is reduced by 17% without increasing gamma. The thinner-plate design conforms to best design practice with a gamma of 0.8 g cm^{-2}; the spine section of 2.24 mm × 1.20 mm is substantially smaller than existing designs. A higher gamma is, however, used for the thin-plate design; 20% of spine metal is removed and this increases gamma to 1.21 g cm^{-2}.

The use of optimized alloy and casting conditions result in a metal structure that is sufficiently resistant to corrosion and creep, so that spines are still in a good condition at the end of life testing, i.e. 1100 cycles with 80% discharge at $C_5/5$. With greater metal saving and higher gamma, however, 'thin-plate' design cells exhibit a reversible loss of available capacity on successive discharge cycles. The available capacity repeatedly declines to less than 80% of nominal during blocks of 50 cycles, but recovers during periods of open-circuit.

4.7. Negative active-material expander

Negative plates that used a commercial formulation, which included Vanisperse organic and mainstream additive levels, showed no performance or cycle endurance problems when low charge-factor charging was used together with an initially appropriate electrolyte saturation. Problems with

the negative active-material may be anticipated under circumstances where the oxygen-recombination current has increased following loss of water from the electrolyte.

4.8. Influence of alloy and processing

Following the recommendation of Albert et al. [2], the tin content of the lead−tin−calcium (0.08 ± 0.01 wt.%) alloy was increased to 1.2 ± 0.1 wt.% for production of positive spine castings. The castings have a fine structure that was resistant to penetrating corrosion. Mechanical, corrosion and creep characteristics are sufficient for the small section components to be in robust condition after long cycle-life. The high-tin alloy is not able, however, to overcome reversible capacity loss in the high gamma thin-plate design.

The performance of the thin-plate, tubular battery represents a substantial improvement for applications that require a high specific energy, e.g. EV duties. The introduction of elliptical-sectioned spines to reduce the gamma value is the reason for improved cycle performance and charge efficiency. This strategy has already been adopted in a new commercial range of antimony-free tubular batteries.

References

[1] D. Pavlov, J. Power Sources 53 (1995) 9–21.
[2] L. Albert, A. Chabrol, L. Torcheux, Ph. Steyer, J.P. Hilger, J. Power Sources 67 (1997) 257–265.
[3] D. Berndt, Maintenance-Free Batteries, Research Studies Press, Taunton, England, 1997 (Sections 8.3 and 13.1.4).
[4] EUCAR Traction Battery Group, EV Battery Test Procedure, December 1996, Appendix N (ECE15L).
[5] E. Meissner, E. Bashtavelova, A. Winsel, in: Proceedings of the 30th ISATA, 97EL066, pp. 127−134.
[6] K. Peters, A.I. Harrison, W.H. Durant, J. Power Sources 2 (1968) 1–16.
[7] H. Döring, in: Brite Euram Project BE97-4085 'Strategies for the Further Improvement of Performance and Life of Lead–Acid Batteries for Electric Vehicle Applications,' Final Technical Report, Appendix V (Task 2b).